Looking for the dM in sdB+dM Systems

Undergraduate Honors Research Thesis

Presented in Partial Fulfillment of the Requirements for Graduation with

Distinction in Astronomy in the Undergraduate College of Mathematical and

Physical Sciences of The Ohio State University

By

Zachary David Hartman

The Ohio State University

May 2015

Project Advisor: Dr. Donald Terndrup

Abstract

We report eclipse timings and optical/infrared photometry of a sample of binary stars that include low-mass, nondegenerate stars, some of which are post-common envelope (PCE) secondary companions to hot subdwarf B (sdB) stars. We model the reflection effect in the later systems to characterize the temperature of the heated hemisphere of the secondaries, first from blackbody fits and then by comparison to libraries of the spectral energy distribution of dwarf M stars. We explore how consistent our phenomenological results are with the properties inferred from analysis of light curve shapes. Currently, the masses of these low-mass stars are unknown. We discuss the prospects for turning these reflection effect systems into double-lined spectroscopic binaries for characterization of the mass-radius relationship of low-mass PCE secondaries.

Table of Contents

List of Tables

List of Figures

Chapter 1: Introduction

HW Virginis binaries consist of a hot ($T_{\text{eff}} \sim 30{,}000$ K), evolved subdwarf B (sdB) star and a cool, low mass main sequence companion, commonly thought to be a dwarf M (dM). These sdBs are extreme horizontal branch stars that have a helium burning core surrounded by a thin layer of hydrogen. HW Vir systems are known to have very short periods (≤ 0.1 days), which means that their orbits should be circularized and the stars should be tidally locked. These systems also exhibit a reflection effect due to the illumination of the dM by the sdB, which causes the hemisphere of the dM facing the sdB to become heated. This effect manifests itself as a sinusoidal variation in the light curve.

Explaining the formation of sdB stars is difficult as the sdB needs to have an extremely thin (< 0.1 $M_\odot$) hydrogen envelope to produce the observed hot temperature. Mengel et al. (1976) was the first to propose close binary evolution as a way for these stars to form. Later, Han et al. (2002, 2003) conducted a binary population synthesis study that expanded upon Mengel et al. (1976) and identified three production channels. The first two include either two main sequence stars or a main sequence star and a white dwarf. As the main sequence star evolves, its envelope expands until mass transfer occurs and a common envelope (CE) binary is formed. In the first channel, envelope ejection occurs and the stars move closer together. For et al. (2010) named this the CE ejection channel, and this mechanism is responsible for forming binaries with periods of ≤ 10 days. The second channel occurs if the mass transfer is stable and the evolved star loses most of its mass to its companion. In this case, a long period binary is formed of $\approx$ 10-500 days and the companion becomes more massive. The final channel for sdB formation occurs if two helium white dwarfs merge and the resulting star is large enough for helium to burn in the core (Han et al. 2002, 2003). The stars that form from this channel

have larger masses than normal sdB stars with $0.4 - 0.65 M_\odot$. However, neither Han et al. (2002, 2003) or Mengel et al. (1976) examine what happens to the low mass secondary during the CE phase. As the mass of the sdB star has changed, the same could have occurred for the secondary in the system. For the systems in our study, we believe they were formed through the CE ejection channel as the predicted masses of the secondary star are around 0.1 $M_\odot$ (Drechsel et al. 2001; Kilkenny et al. 1998; For et al. 2010).

There is little information on the physical state of the cool secondaries as they have only been detected through the strong reflection effect. Because of this, almost all short period post common envelope (PCE) sdB+dM systems are single lined spectroscopic binaries. Several papers (Drechsel et al. 2001; Kilkenny et al. 1998; Vučković et al. 2007; For et al. 2010) have attempted to use light curve modeling codes to find the parameters of the stars in these binaries. However, as little information was available on the secondary, the codes had to be constrained using additional spectroscopic and theoretical information to allow the code to converge. Vučković et al. (2007) and For et al. (2010) attempted this for PG 1336 and 2M 1533 using two different modified versions of the Wilson-Devinney code. Vučković et al. (2007) had to fix the temperature of the secondary to 3,000 K to get the albedo of the secondary to be less than one ($A_{sec} = 0.92$). However, even when the code converged, they had multiple solutions, which were caused by the correlation between several parameters. Vučković et al. (2007) had three solutions and was not able to narrow it down until Charpinet et al. (2008) derived a sdB mass through asteroseismology. For et al. (2010) experienced the same problems for 2M 1533. They attempted to fix the albedo to one. When that failed to give a result, they allowed the albedo to be a free parameter in order for the code to converge. Once it had converged, For et al. (2010) had five possible solutions which they then had to narrow down using the fact that the mass of the sdB should be $\gg 0.08$ $M_\odot$. In their published solution, For et al. (2010) found that their albedo for the secondary was 2, which is unphysical. As a result of these constraints and unreal results, the properties of the secondaries in these systems are poorly constrained. For et al. (2010) derived a temperature for the secondary of 3100 ± 600 K. Drechsel et al. (2001) computed a secondary temperature of 2900 ± 600 K for HS 0705, where they

also constrained A_{sec} to one. These results imply that the secondary contributes little light to the overall flux from the system.

It is possible that these secondaries are inflated from the illumination by the sdB. For et al. (2010) compared their results to the theoretical relations for low mass stars from Baraffe & Chabrier (1996). Using their derived mass of 0.113 $M_\odot$, For et al. (2010) found that the values of T_{eff} and radius from their light curve solution were larger than the values found from the relations of Baraffe & Chabrier (1996). This is in agreement with Irwin et al. (2009) who found that the mass-radius relations for low mass stars under-predict the radii. Kraus et al. (2011) and Feiden & Chaboyer et al. (2012) examined why the models under predict the radii and both came to similar conclusions. All the systems studied by Kraus et al. (2011) and Feiden & Chaboyer et al. (2012) had signs of high chromospheric activity, including star spots and Hα emission. Both point towards the rotation of these stars driving the magnetic activity in these systems. These spots result in the star becoming inflated as it tries to emit the same amount of flux as it would without spots. This could cause the difference between the models and the observed radii as explained in Chabrier et al. (2007). This effect could also be operating in HW Vir systems, where the stars are tidally locked and have period of ~ 0.1 days. In addition to this, the models do not take illumination into account and so the radius might even larger at a given mass than dM stars in the field. The possibly large magnetic activity, coupled with the fact that illumination is not considered, are most likely the two reasons these mass-radius relations do not work for HW Vir systems.

We are engaged in a study to provide better estimates of the dM stars in these systems through time-domain spectroscopy. In this thesis, we present multicolor optical/infrared photometry which allows us to construct the spectral energy distributions of the dM's illuminated hemisphere in three HW Vir binaries and give estimates of the average temperatures. We then comment on the prospects for an observing run designed to get spectra of the secondary. In addition to this, we report new eclipse timings for these systems. Many HW Vir systems have been known to have some form of a period change. We examine our three systems, derive new periods for each plus CM Draconis and look for signs of a period change. We

also report possible time delays in the secondary eclipses due to eccentricity and the Rømer delay using CM Draconis as a baseline.

Chapter 2: Data Reduction and Analysis

2.1. Previous Results from the Literature

HS 0705+6700 was initially found as part of the Hamburg Schmidt Quasar Survey. It was later classified as a short period eclipsing binary by Drechsel et al. (2001), who determined the period of the system to be 0.09564665 days. Between 2001 and 2007, Niarchos et al. (2003), Nemeth et al. (2005) and Kruspe et al. (2007) published eclipse times for HS 0705 but no updated ephemeris was published. Qian et al. (2009) published a large set of eclipse times and conducted an analysis of the eclipse timings. He found that the period appeared to be undergoing a cyclical change and attributed this change to a third body with a period of 7.15 years. As discussed in Qian et al. (2009), HJD 2451957.5274 and HJD 2454706.50400 were not used as they showed large scatter when compared to the rest of the eclispe times. More times were added by Qian et al. (2010), Çamurdan et al. (2012), Beuermann et al. (2012), and Qian et al. (2013). Pulley et al. (2015) was the latest analysis on HS 0705. In addition to adding more timings, Pulley updated the period and looked for signs of an additional period change besides the cyclic change caused by the planet. Table 2.1 shows the quadratic ephemeris from Pulley et al. (2015).

PG 1336-018 was first observed by Kilkenny et al. (1998). Its period was determined to be 0.1010174 days. Kilkenny et al. (2000) observed it again and noted a possible $\dot{P}$. Vučković et al. (2007) published more timings and also conducted an extensive analysis of the light curve to determine the system parameters. Additional timings were gathered by Çamurdan et al. (2012), Qian et al. (2013), Kilkenny et al. (2011) and Lohr et al. (2014). Lee et al. (2014) added a large set of points as well. All of these papers reported a steady $\dot{P}$. Qian et al. (2013) was the first to attribute this change to a planet although they did not rule out angular momentum loss. Lee et al. (2014) agreed with this assessment and also discovered a possible fourth body

in the system by looking at the residuals of a quadratic ephemeris. We discuss Qian et al. (2013)'s and Lee et al. (2014)'s conclusions in chapter 3.

2M 1533 was discovered by Kelley & Shaw et al. (2007). The first timings were published by For et al. (2010), who conducted an extensive analysis of 2M 1533. This is discussed in chapter 3. Additional timings were obtained from Liying & Shengbang et al. (2010), Backhaus et al. (2012) and Lohr et al. (2014).

CM Draconis is a dM+dM system with a period of 1.2 days. As a double-lined spectroscopic binary of two fully convective stars, it is an important tool for testing models. There are few papers with eclipse timings on the system. The first set was published by Lacy et al. (1977). Deeg et al. (2008) published additional timings and studied what appeared to be a period change occurring in the system. Morales et al. (2009) is the most recent eclipse timings study, in which they find that the system is undergoing apsidal motion.

Previous periods and $\dot{P}$ for our four systems are in Table 2.1.

2.2.   Observations and Reduction

Infrared photometry of the three sdB+dM systems was obtained in several runs from 2009 to 2011 using the OSIRIS imaging spectrograph (Depoy et al. 1993) on the 2.4m Hiltner telescope at the MDM observatory at Kitt Peak, Arizona. Exposure times in the JHK filters ranged from 45 s to 90 s, depending on the brightness of the target. The telescope position was dithered slightly between exposures so that we could construct a running median image for sky subtraction and flat fielding.

Optical photometry for the HW Virginis sytems and CM Draconis was obtained from 2011 through 2014 using the 1.3m telescope at the MDM Observatory. Image processing followed the standard procedure of overscan correction and flattening through twilight flat images. Table 2.3 lists the individual time series for each target, and displays the length of time a system was observed and the average cadence.

2.3. Analysis

For the three sdB+dM systems and CM Draconis, differential magnitudes were obtained by taking the weighted average of several comparison stars and subtracting this from the magnitude of the sdB+dM system. Errors were found for these differential magnitudes using error propagation and scaled to the scatter seen in each light curve. The full light curves are shown in Figures 2.1, 2.2 and 2.3. For CM Draconis, errors for some of the light curves were estimated entirely from the variance in the photometry to check the accuracy of error estimates. The differential magnitude of each comparison star was computed with respect to the average of the other comparison stars. The reciprocal of the standard deviation of these differential magnitudes squared was taken to be the weights in a weighted average of the comparsion stars. This was then subtracted off from CM Draconis' magnitude to determine the differential magnitude. The errors for CM Draconis' differential magnitudes were set equivalent to the scatter.

Each light curve was examined and any outliers were excluded from further analysis. The primary and secondary eclipses were then isolated from the rest of the light curve and fit using a scaled Levenberg-Marquardt method with a Gaussian. As we are just looking for the eclipse timings and not modeling other aspects of the systems besides the reflection effect, a simple Gaussian fit is all we need. Once the mid-eclipse times were found, they were converted to BJD(TDB) using the method outlined in Eastman et al. (2010). The results of this fit are shown in Table 3.2.

We isolated the reflection effect data from the light curves by removing the data points we had used to find the eclipse timings. These points were then phased by filter. For each system, we used the ephemeris which was best described by the residuals. A linear ephemeris derived from our eclipse timing analysis was used for 2M 1533, while a quadratic ephemeris was used for PG 1336. As our analysis of HS 0705 is not yet complete, we used a linear ephemeris to phase the light curves. These phased light curves were then fit with a sine function using the Nelder-Mead Simplex method. From this fit, we measured the amplitude and the phase of the reflection effect. Our results are discussed in section 3.2.

System	Period (Days)	$\dot{P}$ (days/yr)	Source
HS 0705	0.0956466012 (16)	$5.82(18) \times 10^{-9}$	Pulley et al. (2015)
PG 1336	0.10101596816 (37)	$-3.36(10) \times 10^{-9}$	Lee et al. (2014)
2M 1533	0.1617704531 (9)	-	Backhaus et al. (2012)
CM Draconis	1.26838995 (5)	-	Morales et al. (2009)

Table 2.1. Previous work on binaries studied in this paper. Errors in the last one or two digits are shown in parentheses.

System	Eclipse Number	Eclipse Times (BJD)	Error (days)	Filter
PG 1336	53551.5	2455632.919590	0.00022	J
	53552.0	2455632.969250	0.00006	J
	53552.5	2455633.019540	0.0002	J
	53561.0	2455633.878530	0.00003	H
	53561.5	2455633.928930	0.00014	H
	53562.0	2455633.979410	0.00003	H
	53562.5	2455634.030060	0.00015	H
	53571.0	2455634.888710	0.00001	K
	53571.5	2455634.939240	0.00017	K
	53572.0	2455634.989570	0.00012	K
	53581.0	2455635.898650	0.00005	J
	53590.5	2455636.858910	0.00017	J
	53591.0	2455636.908950	0.00004	J
	53591.5	2455636.960040	0.00012	J
	53592.0	2455637.009800	0.00004	J
	53600.5	2455637.869080	0.00014	H
	53689.0	2455646.808450	0.00001	I
	53689.5	2455646.858880	0.00004	I
	53690.0	2455646.909480	0.00001	I
	53690.5	2455646.959870	0.00004	I

(cont'd)

Table 2.2. New mid-eclipse timings for all systems. Primary eclipses are assigned number N.0, while secondaries are assigned number N.5.

Table 2.2—Continued

System	Eclipse Number	Eclipse Times (BJD)	Error (days)	Filter
PG 1336	53698.5	2455647.768070	0.00007	Hα
	53699.0	2455647.818630	0.00001	Hα
	53700.5	2455647.970270	0.00007	Hα
	53708.5	2455648.778380	0.00008	Hα
	53709.0	2455648.828820	0.00002	Hα
	53709.5	2455648.879200	0.00008	Hα
	53710.0	2455648.929820	0.00001	Hα
	53710.5	2455648.980380	0.00008	Hα
	53718.5	2455649.788550	0.00007	I_c
	53719.0	2455649.838930	0.00001	I_c
	53719.5	2455649.889560	0.00007	I_c
	53720.0	2455649.939960	0.00001	I_c
	53720.5	2455649.990390	0.00008	I_c
	53728.5	2455650.798490	0.00014	V
	53729.0	2455650.849110	0.00002	V
	53748.0	2455652.768410	0.00002	V
	53748.5	2455652.818890	0.00013	V
	53749.0	2455652.869410	0.00002	V
	53749.5	2455652.919890	0.00013	V
	53750.0	2455652.970400	0.00002	V

(cont'd)

Table 2.2—Continued

System	Eclipse Number	Eclipse Times (BJD)	Error (days)	Filter
2M 1533	-3852.5	2454988.705746	0.00023	K
	-3852.0	2454988.786746	0.00004	K
	-3851.5	2454988.867646	0.00013	K
	-3846.5	2454989.676446	0.00008	J
	-3846.0	2454989.757336	0.00002	J
	-3820.5	2454993.882456	0.00018	H
	-3820.0	2454993.963386	0.00005	H
	7207.5	2456777.887057	0.000003	r
	7214.0	2456778.938615	0.00002	r
	7219.5	2456779.828367	0.00002	z
	7220.0	2456779.909253	0.000004	z
	7226.5	2456780.960806	0.000002	r
	7232.5	2456781.931417	0.00001	i
	7244.0	2456783.791738	0.00003	i
	7244.5	2456783.872666	0.000003	i
	7245.0	2456783.953446	0.00002	i

(cont'd)

Table 2.2—Continued

System	Eclipse Number	Eclipse Times (BJD)	Error (days)	Filter
HS 0705	38413.5	2455496.882770	0.00020	J
	38414.0	2455496.930730	0.00009	J
	38414.5	2455496.978970	0.00010	J
	38415.0	2455497.026490	0.00005	J
	38423.5	2455497.837910	0.00049	K
	38424.0	2455497.887940	0.00024	K
	38424.5	2455497.935720	0.00029	K
	38425.0	2455497.982780	0.00014	K
	39853.5	2455634.614410	0.00012	H
	39854.0	2455634.662300	0.00006	H
	39854.5	2455634.709850	0.00011	H
	39855.0	2455634.758310	0.00007	H
	39855.5	2455634.804730	0.00014	H
	39864.0	2455635.618670	0.00010	J
	39874.5	2455636.622770	0.00020	J
	39875.0	2455636.670810	0.00006	J
	39875.5	2455636.718870	0.00010	J
	39876.0	2455636.766510	0.00005	J
	39885.0	2455637.627270	0.00014	H
	39885.5	2455637.675320	0.00033	H
	39886.0	2455637.723230	0.00017	H
	39886.5	2455637.770420	0.00028	H
	39979.0	2455646.618170	0.00002	I
	39979.5	2455646.666030	0.00005	I
	39980.0	2455646.713810	0.00005	I

(cont'd)

Table 2.2—Continued

System	Eclipse Number	Eclipse Times (BJD)	Error (days)	Filter
HS 0705	39989.5	2455647.622540	0.00004	Hα
	39990.0	2455647.670280	0.00001	Hα
	39990.5	2455647.718220	0.00004	Hα
	40000.0	2455648.626770	0.00001	Hα
	40000.5	2455648.674580	0.00004	Hα
	40001.0	2455648.722370	0.00001	Hα
	40010.5	2455649.631140	0.00010	I_c
	40011.0	2455649.678880	0.00002	I_c
	40011.5	2455649.726880	0.00005	I_c
	40021.0	2455650.635340	0.00002	v
	40021.5	2455650.683440	0.00009	v
	40022.0	2455650.731000	0.00001	v
	40042.0	2455652.643950	0.00001	v
	40042.5	2455652.691840	0.00006	v
CM Draconis	10959.5	2456458.728350	0.00002	Hα
	10962.0	2456461.900552	0.000005	r
	10965.0	2456465.705708	0.000005	r
	10967.5	2456468.875490	0.000008	r
	10969.0	2456470.779313	0.000005	r
	11213.5	2456780.899483	0.000006	r
	11215.0	2456782.803147	0.00002	r

System	Filter	Duration (days)	Cadence (days)
2M 1533	H	0.25452220	0.00132564
	J	0.15210500	0.00132265
	K	0.24579140	0.00146304
	i	0.26923700	0.00069213
	i	0.09255780	0.00062119
	r	0.15635450	0.00073752
	r	0.07963410	0.00067487
	r	0.03693750	0.00064803
	z	0.16112170	0.00059019

Table 2.3.   Cadence and duration of observations

Table 2.3—Continued

System	Filter	Duration (days)	Cadence (days)
PG 1336	H	0.05737745	0.00147122
	H	0.18858299	0.00154576
	J	0.03425969	0.00180314
	J	0.24423997	0.00836500
	K	0.19200000	0.00182857
	I	0.20819020	0.00034814
	Hα	0.23691650	0.00034236
	Hα	0.26535620	0.00066505
	I$_c$	0.24816670	0.00034757
	V	0.09304650	0.00042879
	V	0.27066590	0.00043168
HS 0705	H	0.20105231	0.00184452
	H	0.23319690	0.00189489
	J	0.03217084	0.00201068
	J	0.19250797	0.01065724
	J	0.17821400	0.00160553
	K	0.19750760	0.00205737
	I	0.13981570	0.00028075
	Hα	0.14275580	0.00034399
	Hα	0.14666760	0.00028205
	I$_c$	0.11892710	0.00031462
	V	0.13861240	0.00028878
	V	0.09963460	0.00036099

(cont'd)

Table 2.3—Continued

System	Filter	Duration (days)	Cadence (days)
CM Dra	Hα	0.29639236	0.00156821
	Hα	0.28487734	0.00193794
	r	0.30791879	0.00105092
	Hα	0.13046390	0.00191859
	r	0.10293471	0.00103974
	Hα	0.25782272	0.00192405
	r	0.18168750	0.00121125
	r	0.30503117	0.00103752
	r	0.29921994	0.00104258
	r	0.11660900	0.00048995
	r	0.11170610	0.00062406
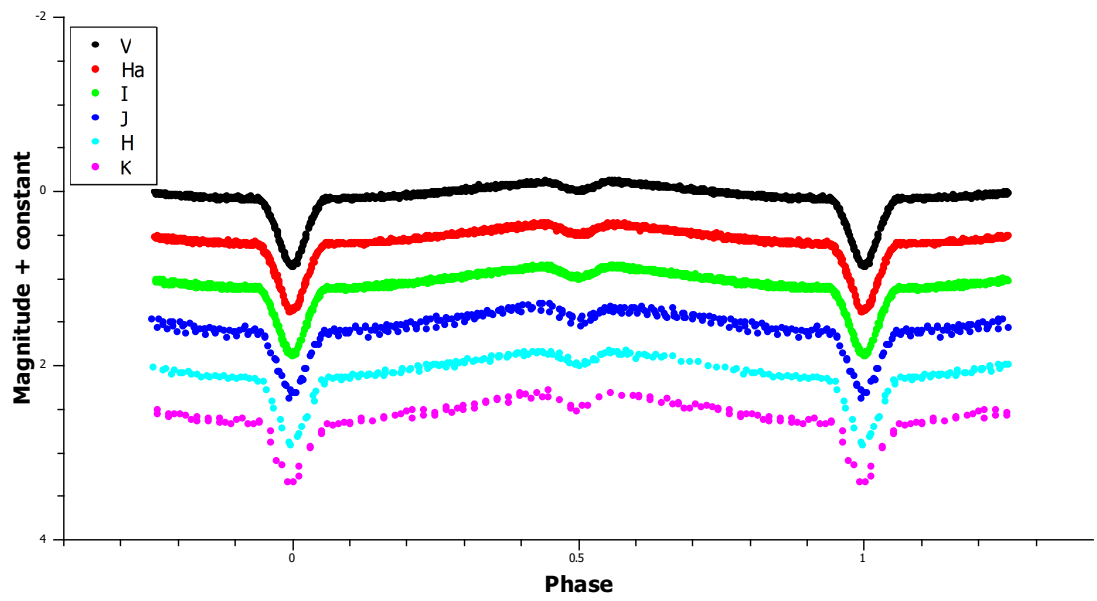
Fig. 2.1.— PG 1336 full light curves. They have been normalized to zero and offset.

17
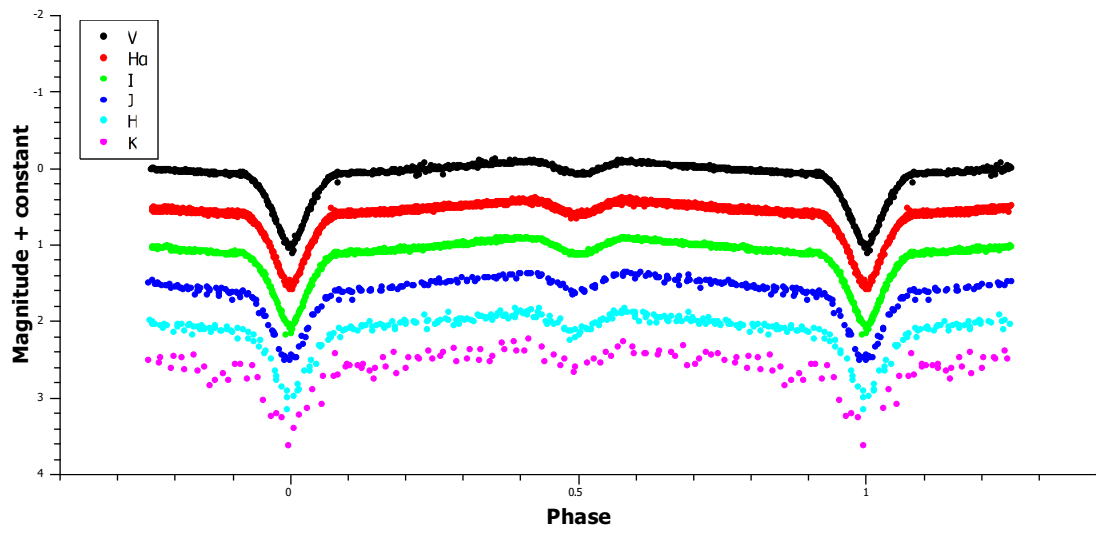
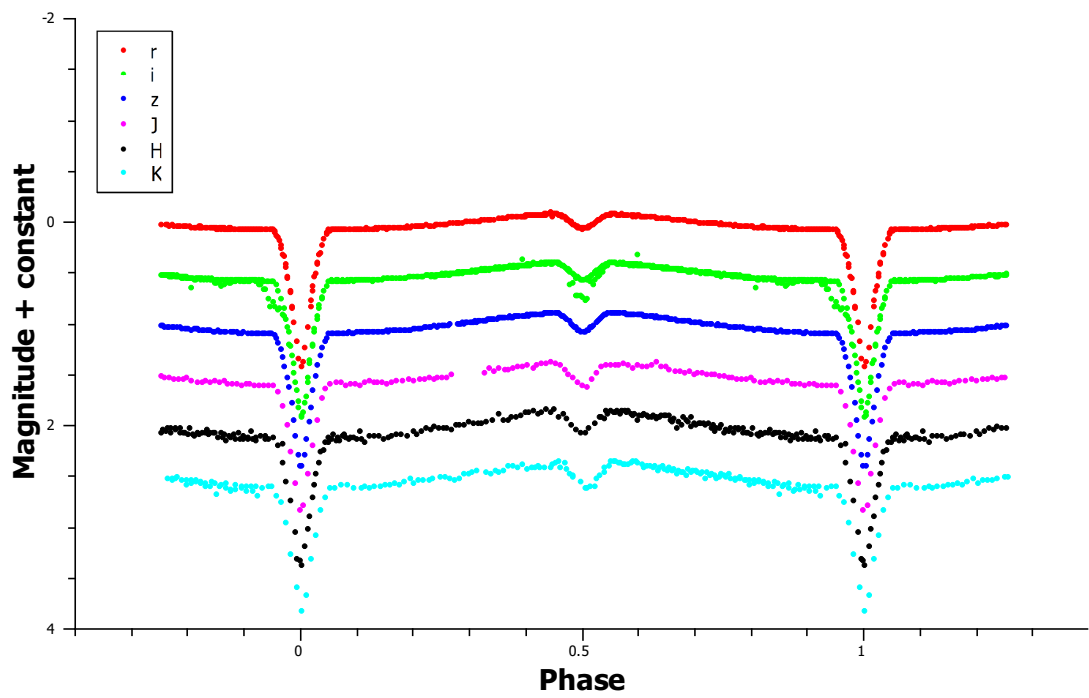Fig. 2.2.— HS 0705 full light curves

Fig. 2.3.— 2M 1533 full light curves

Chapter 3: Eclipse Timing and Reflection Effect Analysis

3.1. Eclipse Timing Study of SdB+dM systems and CM Draconis

For each system, we combined our eclipse timings with times found in the literature, and converted them to BJD(TDB) using the same method as previously discussed for our eclipse times. For CM Draconis, we used the original values from Lacy et al. (1977) instead of the recalculated values from Deeg et al. (2008). Once we had our combined data sets, we took a previous ephemeris and used it to assign each eclipse a number. For 2M 1533, we used Backhaus et al. (2012). For PG 1336, we used the linear ephemeris of Kilkenny et al. (2000). For HS 0705, the ephemeris from Drechsel et al. (2001) was used. For CM Draconis, we first used the ephemeris put forth by Morales et al. (2009). These numbers were then rounded to either N.0 (primary eclipse) or N.5 (secondary eclipse). We then fit each data set using a linear least-squares fit with the equation $T_{min} = T_0 + \eta P$, with T_{min} representing the time of the eclipse minimum, T_0 representing the eclipse minimum at $\eta = 0$, η is the eclipse number and P is the orbital period. We took this fit and constructed an $O\text{-}C$ diagram for each sdB+dM system. These are shown in Figures 3.1, 3.3 and 3.4 for PG 1336, HS 0705 and 2M 1533, respectively.

Looking at Figure 3.1 for PG 1336, a linear fit appears insufficient for the gathered eclipse timings. The $O\text{-}C$ diagram shows that a quadratic ephemeris could achieve better results. We went back and fit the data with the same equation as above except for the addition of a $c\eta^2$ term, where c represented the quadratic change. This c term is related to the actual period change through the equation $c = (P\dot{P})/2$. Table 3.1 shows our results for the quadratic fit to the PG 1336 data set and provides our result for the period change in PG 1336. The errors for these values are slightly better than those in Lee et al. (2014) and the errors in $\dot{P}$ are

smaller by an order of magnitude than Kilkenny et al. (2011). Figure 3.2 shows the O-C diagram for the quadratic ephemeris and highlights that the quadratic ephemeris is a much better fit. The reason for the spread in our data points is because we include new IR photometry. This IR photometry has a much lower cadence than optical photometry which leads to higher errors and more scatter in the residuals. This particularly affects the secondary eclipses that are found in the IR light curves as these eclipses have fewer points than the primaries. This is seen in our O-C diagram.

Figure 3.3 shows the linear O-C diagram for HS 0705. Most of our times are as accurate as other published times, although our IR secondary eclipse timings are worse than the others. There is a clear sinusoidal pattern in the O-C diagram, which indicates a third body. There could also be an unexplained, long term quadratic behavior just like in PG 1336. Many authors have examined this system and have found parameters for the third body, with and without a quadratic term in their fit. Qian et al. (2013) put its period at 9.53 yr if the data was fit without a quadtratic term or 8.87 yr if a quadratic term was included. Pulley et al. (2015) determined similar results for both fits. HS 0705 is still under study as the planet complicates the analysis.

2M 1533's linear O-C diagram is shown in Figure 3.4. Once again, our times compared favorably to the literature data and we extend the span of the available data by a year. Compared to the other two sdB+dM systems studied, this system appears to be best fit by a linear ephemeris. As our other systems appeared to have some period change, we decided to fit a quadratic ephemeris to the data set and see which one fit better by comparing $\chi^2/d.o.f.$. The quadratic fit was slightly better than the linear fit. The $\chi^2/d.o.f.$ for the linear fit was 5.6, while for the quadratic fit, it was 5.4. While this does not definitively prove that the quadratic fit is better, it does show that both are equally valid. Table 3.1 shows our values for P and $\dot{P}$ as found from the quadratic fit as it is slightly better. Our period agrees with that found in Backhaus et al. (2012) and is slightly better than that found in For et al. (2010). This is the 'youngest' of our systems with the first timings on it published in 2010. Our other two systems have timings dating back to the late 1990s. This

relatively small span of data could be the reason for the lack of quadratic behavior in the linear O-C diagram. This was seen in Kilkenny et al. (2000) for PG 1336. If the $\dot{P}$ in 2M 1533 was as large as PG 1336's $\dot{P}$, we should have seen some quadratic behavior in the O-C diagram. It could be that the $\dot{P}$ is smaller in 2M 1533 and, with the addition of more data over the next couple of years, a quadratic trend could begin to form.

Many papers, Qian et al. (2012) and Lee et al. (2014) are two examples, have debated between two causes for the period change in PG 1336. Several sdB+dM systems, such as HS 0705 (Qian et al. 2013) and HW Vir (Lee et al. 2009), are known to have third bodies orbiting them. Lee et al. (2014) explored if this could be occurring in PG 1336. In their paper, Lee modelled PG 1336 in two different ways. They first fit their data set with a quadratic ephemeris plus a term that takes into account the light travel time (LTT) due to a third body. They then assumed that the long term quadratic behavior was caused by another body and so they used a linear equation plus two LTT terms. Using the second method, they found that there were two planets orbiting the binary, one with a period of 8.2 yr and another with a period of 27.0 yr. The 27.0 yr period describes the planet that could be the cause of the long term quadratic behavior, while the 8.2 yr period explains the small sinusoidal variation that appears to be present in Figure 3.2. To check these claims, we used Period04 to look for periodic signals in the residuals between our data and our quadratic ephemeris. Period04 is a free program that can take the fourier transform of a set of data (Lenz & Breger 2004). Our results are shown in Figure 3.5. The frequencies that match to the two peaks seen are 0.000397 and 0.0000815. These frequencies correspond to periods of 6.9 and 33.6 yrs. While these do not match well with Lee's findings, they do support the presence of a third body with a period of < 10 yr. However, we can not determine if another longer period planet is orbiting the system as it has not completed an orbit yet. If a fourth body was around the binary, the O-C diagram with a linear ephemeris should begin to look like Figure 3.3. More observations in the future are needed to test this theory.

Another possibility is that this period change is due to the magnetic activity of the low mass star. Both Qian et al. (2012) and Lee et al. (2014) examined if

the applegate mechanism could be the cause of this change. This mechanism links period modulations to magnetic activity cycles in the low mass star. Applegate et al. (1992) states that if the distribution of angular momentum changes as the star goes through its activity cycle, possibly due to the action of a magnetic torque, the rotational oblateness of the star will change, and this change will be communicated to the orbit by gravity, changing the orbital period. The star is also required to be variable for this mechanism to work and the period of the luminosity variation is equal to the period variation. Lee et al. (2014) stated that that the Applegate mechanism was unlikely as the luminosity variations are too large. Lee et al. (2014) also looked at the possibility of angular momentum loss due to a stellar wind and gravitational radiation being the cause of the large $\dot{P}$ in PG 1336. They determined that gravitational radiation was unlikely due to its magnitude being too small. They did find that the magnitude of a possible angular momentum loss due to a stellar wind was on the same order of magnitude as the observed period change. However, they stressed that because of the fully convective nature of the secondary, magnetic braking may not be the dominant source for the period change. With this in mind, they agreed with Qian et al. (2012) that the most likely possibility for the period change in PG 1336 is due to a planet.

In addition to these sdB+dM systems, we also have new timings for CM Draconis. Figure 3.9 shows the new linear O-C diagram and Table 3.1 shows the period we got from our data set. This period matches with the results from Morales et al. (2009). We also decided to compute a $\dot{P}$ for CM Draconis as a baseline for the sdB+dM systems. We found that the $\dot{P}$ for CM Draconis was zero within the errors. This is different from the findings of Deeg et al. (2008) and Morales et al. (2009). Both reported a period change. Deeg et al. (2008) attributed this to a third body around the system, while Morales et al. (2009) pointed out that there is not enough evidence to support this yet. We agree with Morales et al. (2009) as a linear fit to the data yielded a $\chi^2/d.o.f.$ roughly equal to a quadratic fit. There also appears to be two distinct groups of eclipse timings in Figure 3.9. These represent the secondary and primary eclipses, the top being the later and the bottom being the former. To our knowledge, no analysis has been done on this time difference. Morales et al. (2009) examined the eclipse times for apsidal motion but did not

determine what the time difference between the primaries and the secondaries was. We examined this difference by fitting just the primary eclipses we had with a linear ephemeris and computed the residuals for all the eclipses, secondary and primary, with that ephemeris. We then took the average of the residuals for the secondary eclipses as our time difference. Our value is shown in Table 3.1. This time difference is mostly due to the eccentricity of the orbit of the binary. An excellent discussion of this is found in Kaplan et al. (2010) and Barlow et al. (2012), which does this study on an sdB+dM system 2M 1938. We use equation 2 from Barlow et al. (2012) to describe the time delay due to eccentricity. This equation is

$$\Delta T \simeq ((2Pe)/(\pi)) * \cos \omega,$$

where P is the period, e is the eccentricity and ω is the argument of periapsis. Taking the values of e and ω from Morales et al. (2009) and using the P we found previously, we found that our estimated delay due to the eccentricity would be $\Delta T = -0.00132 \pm 0.00006$ days. This value is very close to our observed value, which reinforces the belief that the delay in CM Draconis is due to the eccentricity of the orbit.

For 2M 1938, Barlow et al. (2012) found a time delay in the secondary eclipses of about 2 seconds, but as 2M 1938 should be circularized, they attributed this delay to the Rømer delay. Using their equation (1), they were able to derive a mass ratio. We took this equation and, using the mass ratios in For et al. (2010) and Vučković et al. (2007) for 2M 1533 and PG 1336, estimated what the Rømer delay would be. This equation is

$$\Delta T_{\text{LTT}} = (PK_{sd}/(\pi c)) * ((1/q) - 1),$$

where K_{sd} is the sdB orbital velocity, q is the mass ratio, c is the speed of light and P is the period. For 2M 1533, we estimated a delay of ~ 2.5 seconds, while for PG 1336, it was ~ 2 seconds. We then used the same procedure as our analysis of CM Draconis and found what the time delays were for both systems. Table 3.1 shows our time delays with errors. Our delays are far from what we predicted. There are three reasons for this. For both systems, the scatter in the secondaries is much greater than the delay we are looking for which could cover up the delay. For PG

1336, the planet with the smaller orbit of 8.2 years is not included in our ephemeris, which would affect the average of the secondaries. For 2M 1533 especially, there is also the problem of too few secondary eclipses. Out of the 282 eclipses for 2M 1533, only 19 are secondary eclipse and several of those are IR secondaries which has extremely high errors and scatter. Because of these factors, our errors are too large to report any definitive detections of the Rømer delay. If more precise secondary timings are taken, then an experiment such as this one could lead to interesting results.

3.2.   Study of sdB+dM Reflection Effect

All of the known sdB+dM systems have been observed to have some reflection effect in the light curves as shown in Figures 2.1, 2.2 and 2.3. We conducted an analysis of this reflection effect over a span of wavelengths including the optical and the IR. Our process was described in Section 2.3 and our results are shown in Table 3.2. As discussed in the introduction, little is known about the secondaries in these systems. However, the reflection effect offers us a way to characterize at least half of the low mass star. The peak to peak amplitude of the reflection effect should represent the difference between the flux of both stars combined and flux from just the primary. If we write the magnitude equation as

$$\Delta m = m_{prim+sec} - m_{prim} = -2.5 Log((F_s + F_p)/(F_p)),$$

and use the peak to peak amplitude as Δm, we get the ratio of the flux of the secondary to the flux of the primary. Table 3.2 shows our results. We observed that as we looked at redder filters, F_s/F_p becomes larger. This makes sense as low mass stars produce more flux in that wavelength range compared to the hot sdB which produces more flux at bluer wavelengths. The flux ratio provided us with a way to model the spectral energy distribution of the low mass star. By assuming that the reported magnitudes for these systems were the magnitudes of just the sdB star, we had the flux of the primary. Combined with the flux ratio, we managed to derive a way to get an estimated flux of the secondary. Figure 3.6 shows the results of our calculations for PG 1336 and Figures 3.7 and 3.8 show results for HS 0705 and 2M

1533. Based on other studies, such as For et al. (2010) and Vučković et al. (2007), we expected the distribution to look like that of a 3,000 K blackbody plus reflected light from the sdB. We found what appears to be a cooler mirror of the sdB for all three of our sdB+dM systems. In all three cases, we found that the expected temperature of the heated hemisphere of the low mass star was around 10,000 K after being fit with a blackbody model with two variables, temperature and a constant representing the ratio of the radius of the star being fitted over the distance. Our temperatures and errors are reported in Table 3.4. Our sdB temperatures nearly match those found from fitting models to the Balmer lines in the spectra as described in For et al. (2010), Drechsel et al. (2001) and Vučković et al. (2007). We find that 2M 1533's secondary is the coldest of the three, which is reasonable as it is the widest binary. We also find that for the three systems studied, the primary and the secondaries have very similar radii. This was found by taking the ratio of the constant in the blackbody fits of the primary and the secondary in each system. For 2M 1533 and HS 0705, they are the same size while the radius ratio for PG 1336 is 0.76. Other papers have attempted to put forth ideas as to what is going on in these low mass stars. The prevalent explanation is that thermalization and re-radiation is occurring on the heated side of the secondaries without heat redistribution. We see this in the spectral energy distributions as the spectrum should look like a blackbody with a radius equal to that of the sdB, but with a cooler temperature. This would allow for the strong reflection effect and for the shape of our distributions.

These high temperatures also imply a couple of critical points when attempting to model these systems. Because of this strong reflection effect, the models being used to model the light curves for these binaries need to be reworked as well. We see this in For et al. (2010) where their model only works if their albedo becomes two or other papers, like Vučković et al. (2007), where the temperature of the secondary had to be fixed and they reported an albedo of 0.92. Budaj et al. (2011) points out that the reflection effect, especially the albedo, in these models must be rethought. As described by Budaj, the albedo in the Wilson-Devinney code is described as a bolometric albedo. This albedo is the fraction of impinging energy that is converted to heat, raises the temperature and is re-radiated. Budaj et al. (2011) discusses that there could be a significant amount of energy that is not absorbed but reflected or

scattered. This needs to be taken into account in these models. The SHELLSPEC code (Budaj et al. 2011) does this and we are in the process of familiarizing ourselves with it. With this code, we are able to explore the possibility that instead of immediate re-radiation, there is significant reprocessing of the heat. An albedo of one in the Wilson-Devinney code means that all the energy hitting the surface is thermalized and it is entirely possible that the star redistributes the heat gained through this process instead of re-radiating it. This would occur if the timescale for heat transfer was less than the timescale for re-emittance. The circulation of the heat could also lead to the formation of rings of different temperatures spanning from a central hotspot to the other side of the secondary. In our analysis of the spectral energy distributions, we computed the average temperature of the heated hemisphere. Time-domain spectroscopy would be able to see if these rings were present on the secondary.

Our spectral energy distributions provides us with the ability to examine the prospects of an observing campaign designed to detect the secondary's spectra. Two attempts have been made at detecting the secondary. Vučković et al. (2007) attempted to see the spectra of the secondary in PG 1336 but their S/N was too low. Wood & Saffer (1999) saw absorption lines when emission lines were expected (For et al. 2010) but were still able to derive a radial velocity for the secondary. Both of these papers looked in the optical, where the sdB is supposed to dominate the flux emitted by the system. Based on our study, the secondary contributes more light in the red filters than in the blue. If we look in the red, we could see the spectra of the low mass secondary. It is more likely, however, that we would detect the heated hemisphere in such an observing run. According to our study, the illuminated side should have a temperature of around 10,000 K. If the spectra of the secondary is seen, then a radial velocity study could still be attempted, which would yield the mass of the low mass secondary. This would allow us to set up a mass-radius relation for these secondaries, making future modeling more accurate. We would be able to find the density of these systems to examine how the common envelope affected them and allow us to examine the temperature distribution on the heated hemisphere of the secondary.

Illuminated exoplanets offer an interesting comparison for HW Vir systems as they are experiencing the same reflection effect. Zellem et al. (2014) finds that the hotspot on the exoplanet is not in phase with the eclipses, indicating some circulation on the planet. As seen in Zellem et al. (2014), the eclipses for HD 209458b occur much later in the light curve than the peaks of the reflection effect. Table 3.3 shows that our three systems do differ slightly from being perfectly in phase with the reflection effect. Zellem et al. (2014) points out that high opacity leads to a smaller phase difference. As the secondaries in our systems should have a high opacity, they should also have a smaller phase difference as is seen. The opacity in these systems could also be higher because they could have high metallicity (Zellem et al. 2014). As a result of how these systems formed, helium contained in the common envelope could have been transferred to the secondary. When the envelope dissipates, the helium could remain on the secondary. This would drive up the metallicity, increase the opacity and keep the phase difference small.

3.3.   Future Work

As has been stated, little is known about the low mass stars. We know the radii, we know they are strongly illuminated and we know that they contribute more light in the IR. We also know that the models give poorly constrained results for the secondaries. The next step is to get spectra on the low mass stars. Only a couple of people have tried because of the difficulty of the task. We plan on being the next group to try to see the secondary by taking spectra in the wavelength range 5000-9000 $\mathring{A}$. As the secondary contributes more light in this region than in a region > 6000 $\mathring{A}$, this is our best chance to detect it. We will be taking spectra throughout the orbit but we will be specifically focusing on the time between quarter phase and the secondary eclipse. This is the time when the hot hemisphere of the secondary will be facing us and offers the most likely chance for detection. We would then subtract off spectra taken of the primary to see if we can find lines from the secondary. The SHELLSPEC code allows us to predict what the phase-resolved spectra of this system might look like and allows us to better plan the observing run. Lines of interest include Hα, the Ca II triplet and some of the Paschen lines.

If detected, this would set up a run at the Large Binocular Telescope, where radial velocity data could be gathered. That data would allow us to find the mass of the secondary and reach our ultimate goal of putting these heavily illuminated objects on a mass-radius relation.

3.4. Conclusion

We have reported new eclipses timings for three short period PCE sdB+dM binaries and one dM+dM system. Through a careful analysis for the eclipse timings, we have concluded that there is a steady $\dot{P}$ in PG 1336 and possible $\dot{P}$s in 2M 1533 and CM Draconis. We also examined these systems for evidence of a time delay between the secondary eclipses and expected eclipse time. We found that CM Draconis has a significant time delay due to the eccentricity of its orbit, while PG 1336 and 2M 1533 show possible signs of the Rømer delay. A detailed examination of the reflection effect in these systems led us to characterize the spectral energy distribution of the heated hemispheres of the low mass secondaries. This analysis allowed us to speculate on the potentials of an observing run to try and see the spectra of the secondary, something which has not been done adequately yet. We will be going on an observing run to attempt to see the spectra in the infra-red in May 2015. If successful, this would allow us to move on in our plan to ultimately get the masses of these low mass secondaries and learn more about what is going on in these heavily illuminated stars.

System	Period (Days)	$\dot{P}$ (days/yr)	$\Delta\,T_{secondaries}$ (s)
HS 0705	0.09564673372 (3)	-	-
PG 1336	0.1010160030 (4)	$-4.48(4) \times 10^{-9}$	7.0 (1)
2M 1533	0.1617704548 (5)	$1.3(2) \times 10^{-9}$	1.0 (2)
CM Draconis	1.268389985 (5)	$-0.1(4) \times 10^{-10}$	-101.3 (7)

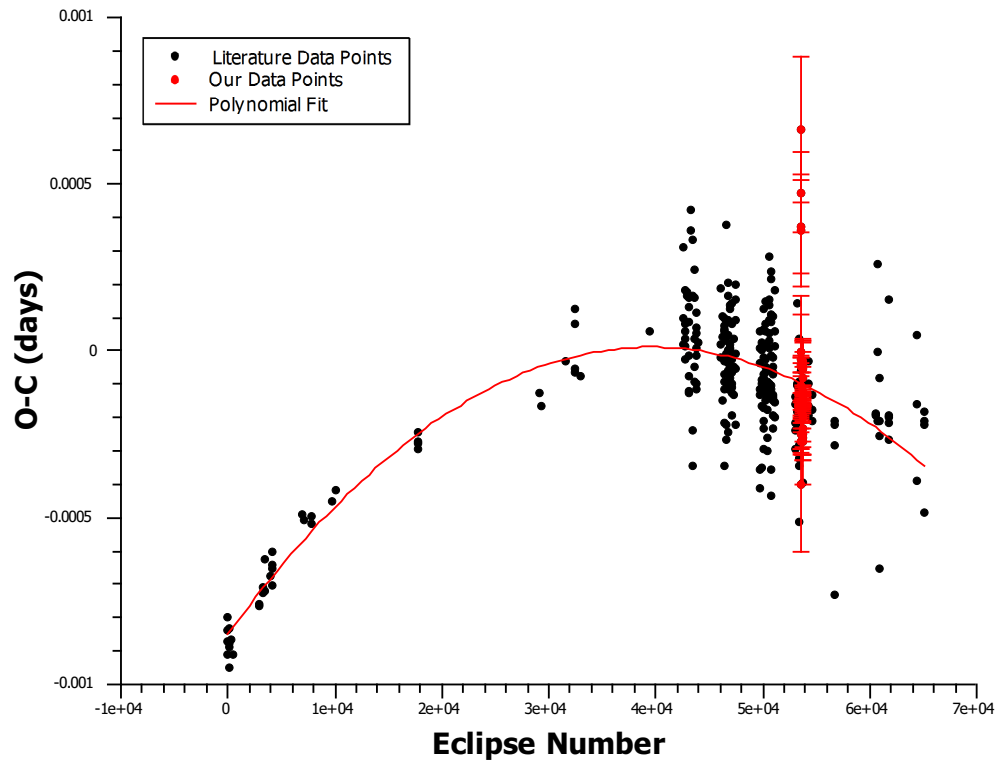Table 3.1.   Binaries analyzed in this paper. Numbers in parentheses represent error in last digit.

Fig. 3.1.— PG 1336 O-C with respect to a linear ephemeris. Errors in Literature data points are roughly equal to the scatter.

System	Filter	Peak to Peak Amplitude (Mag)	Error	F_{Sec}/F_{Prim}	Error
2M 1533	B	0.1	0.0004	0.0965	0.0004
	V	0.13	0.0004	0.1272	0.0003
	r	0.1642	0.0004	0.1633	0.0003
	R	0.15	0.0004	0.1482	0.0003
	i	0.2018	0.0004	0.2043	0.0003
	z	0.2174	0.0006	0.2217	0.0005
	J	0.224	0.004	0.229	0.003
	H	0.272	0.006	0.285	0.004
	K	0.272	0.006	0.285	0.004
HS 0705	V	0.18	0.01	0.183	0.008
	Hα	0.2126	0.0014	0.216	0.001
	I	0.230	0.002	0.236	0.001
	J	0.270	0.006	0.282	0.004
	H	0.216	0.004	0.220	0.003
	K	0.32	0.04	0.34	0.03
PG 1336	V	0.208	0.002	0.211	0.002
	Hα	0.250	0.002	0.259	0.001
	r	0.250	0.002	0.259	0.001
	I	0.278	0.001	0.292	0.001
	J	0.328	0.004	0.353	0.003
	H	0.328	0.004	0.353	0.003
	K	0.36	0.01	0.393	0.008

Table 3.2. Reflection effect in sdB+dM systems

System	Filter	Phase	Error
2M 1533	r	1.581	0.002
	i	1.600	0.001
	z	1.571	0.002
	J	1.57	0.01
	H	1.56	0.02
	K	1.55	0.02
HS 0705	V	1.625	0.005
	Hα	1.575	0.003
	I	1.615	0.005
	J	1.59	0.01
	H	1.67	0.01
	K	1.68	0.04
PG 1336	V	1.568	0.008
	Hα	1.509	0.004
	I	1.571	0.003
	J	1.567	0.006
	H	1.603	0.009
	K	1.57	0.02

Table 3.3.   Phase of sdB+dM systems between eclipses and reflection effect

System	sdB Temperature	Error	dM Temperature	Error
2M 1533	29,200	200	10,600	70
HS 0705	28,800	400	12,000	200
PG 1336	31,300	200	13,600	200

Table 3.4. Temperature of sdB and dM determined from Blackbody fits to spectral energy distribution
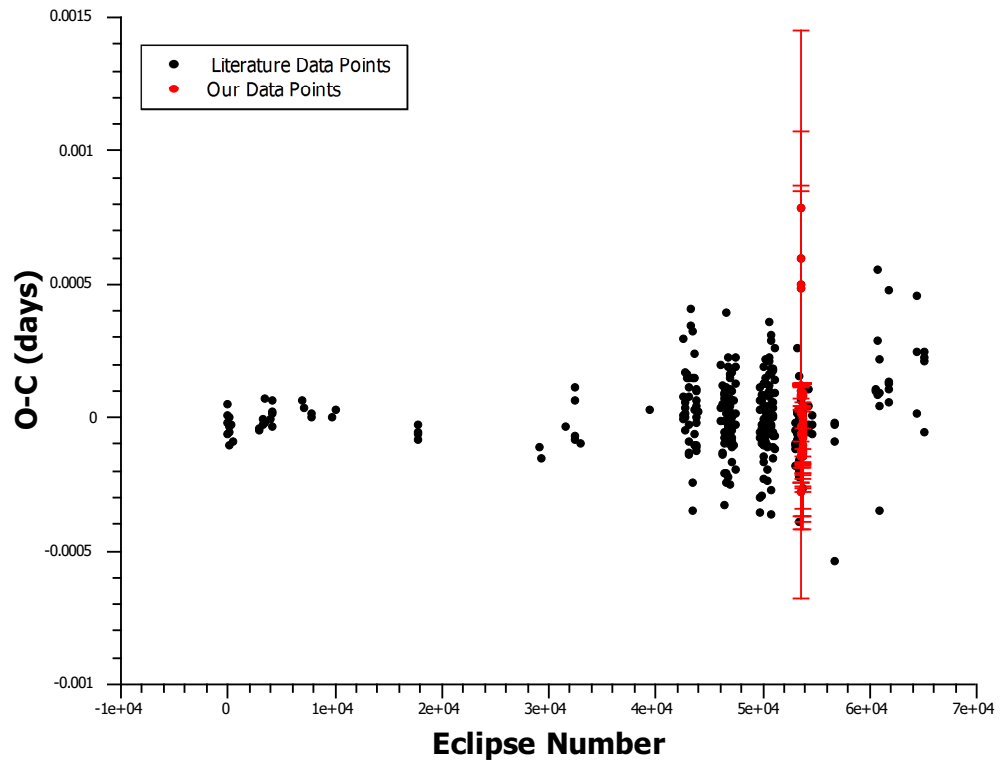
Fig. 3.2.— PG 1336 O-C with respect to a quadratic ephemeris
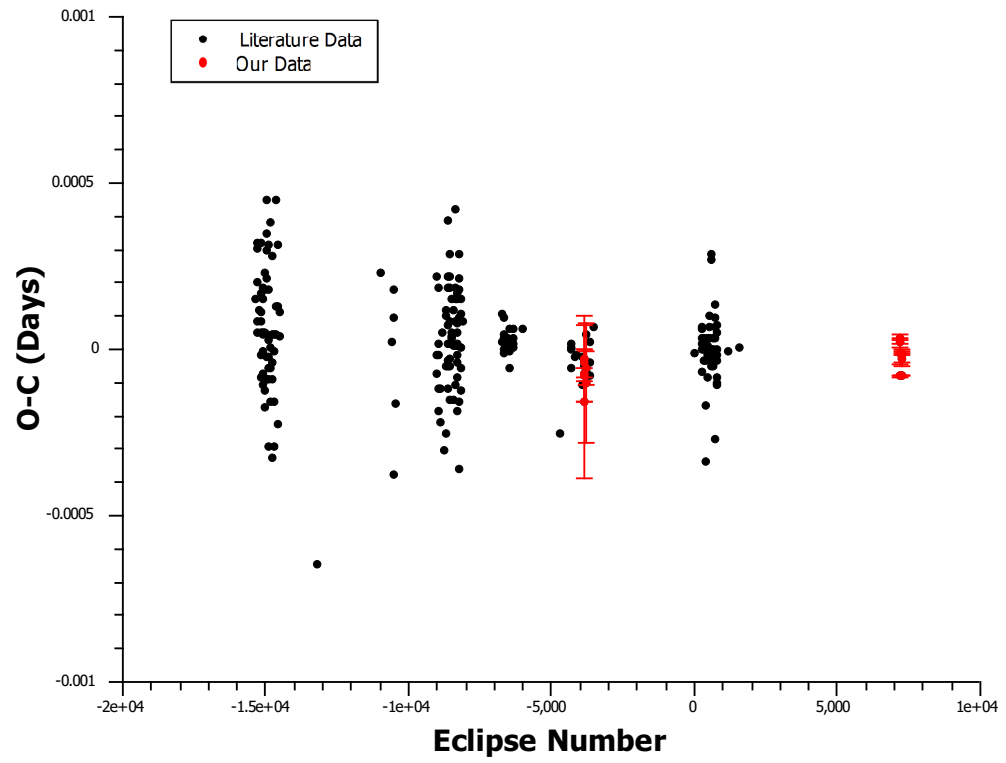
33
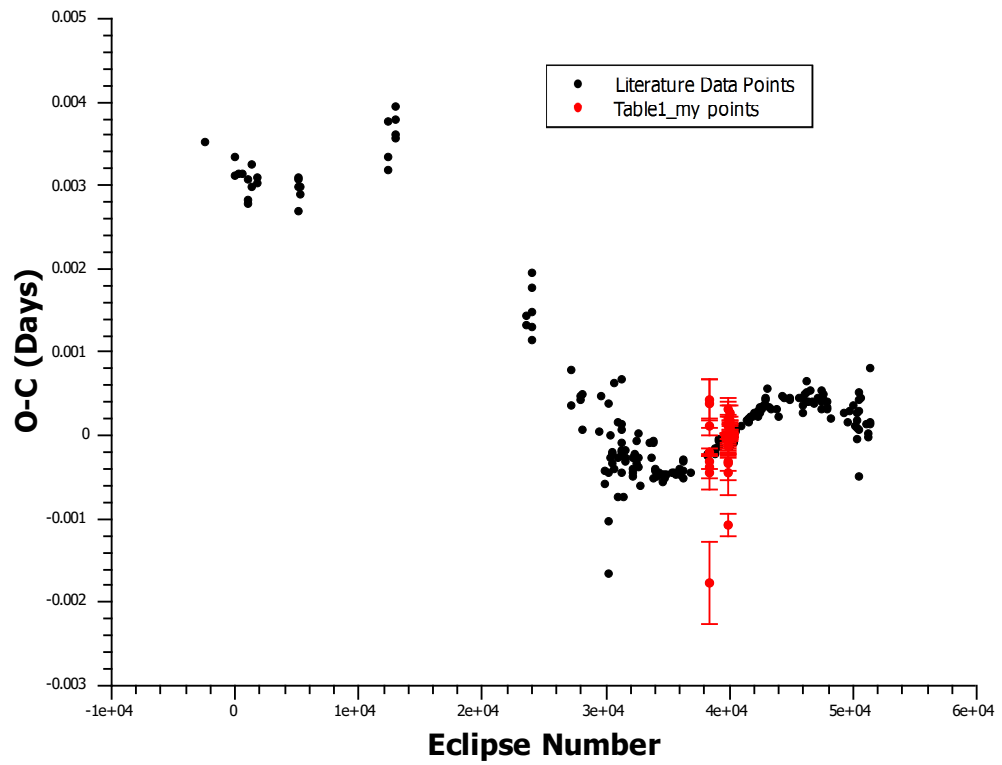
Fig. 3.3.— HS 0705 O-C with respect to a linear ephemeris

Fig. 3.4.— 2M 1533 O-C with respect to a quadratic ephemeris
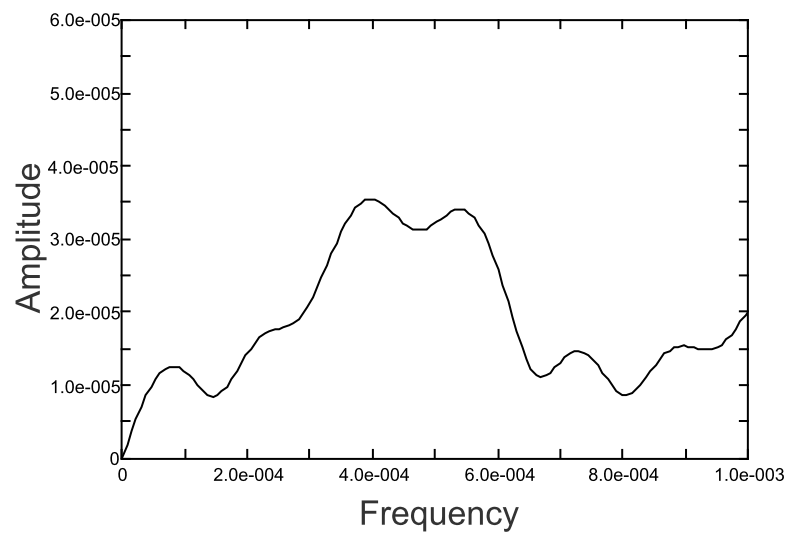
Fig. 3.5.— Period04 fourier transform plot for PG 1336
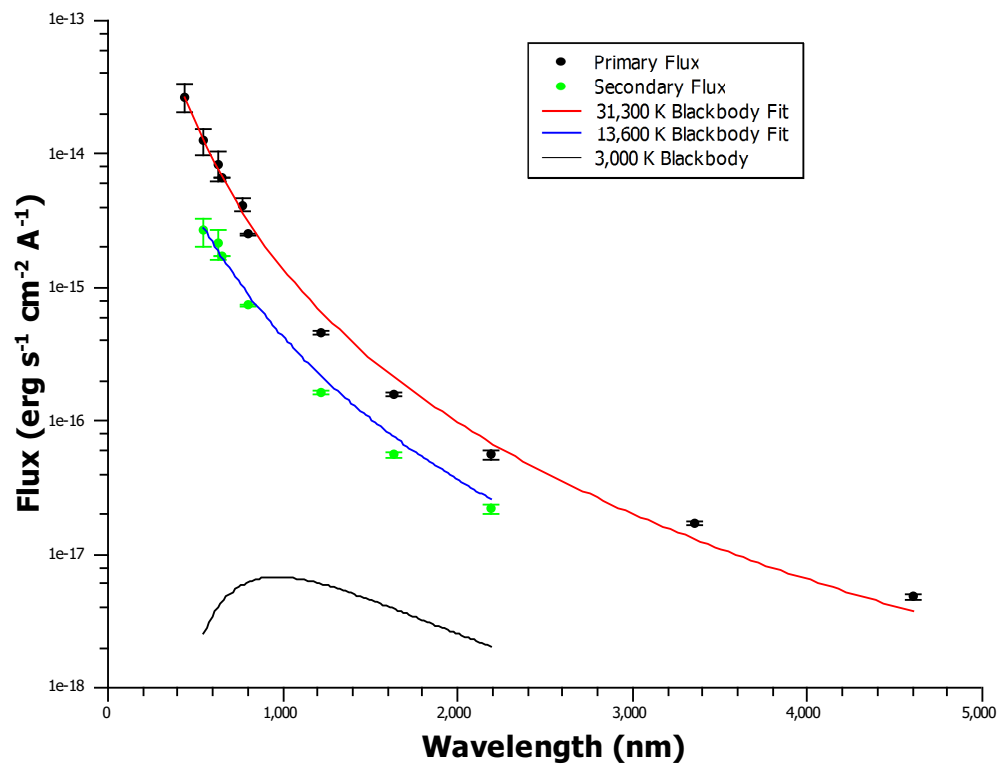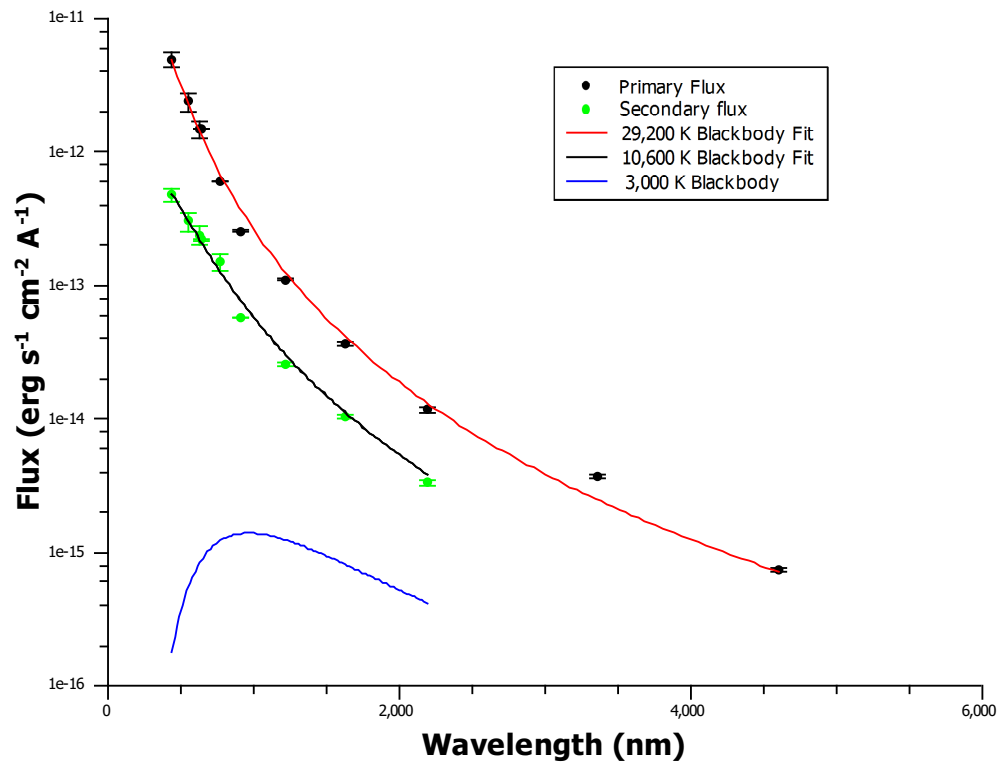
Fig. 3.6.— PG 1336 spectral energy distribution

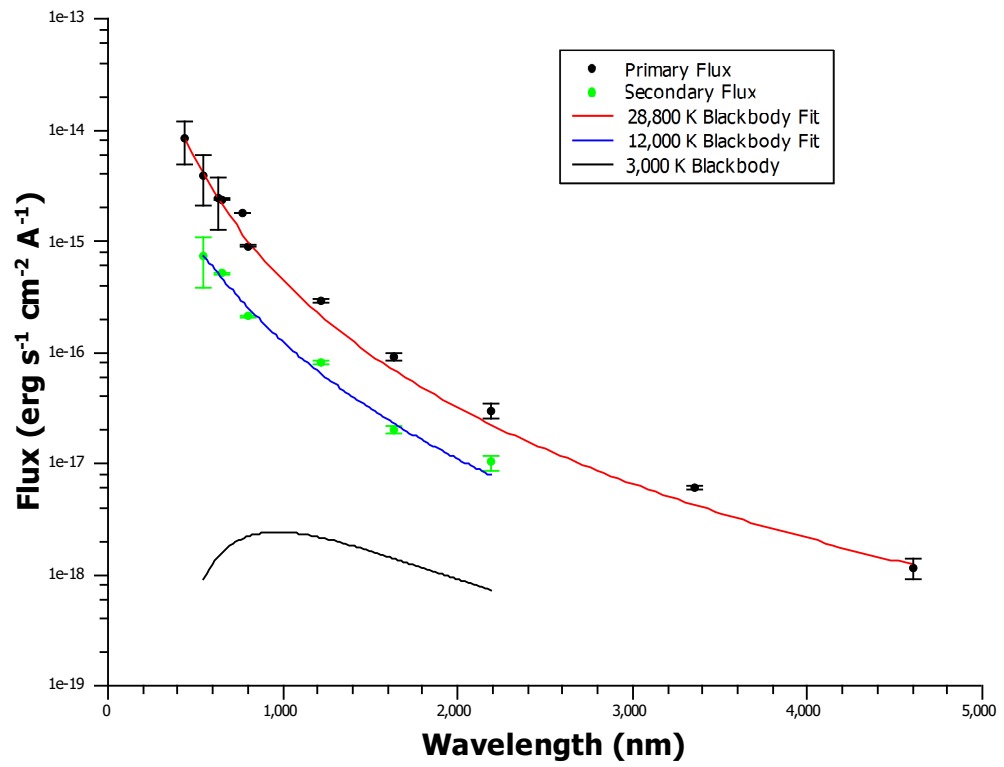Fig. 3.7.— 2M 1533 spectral energy distribution

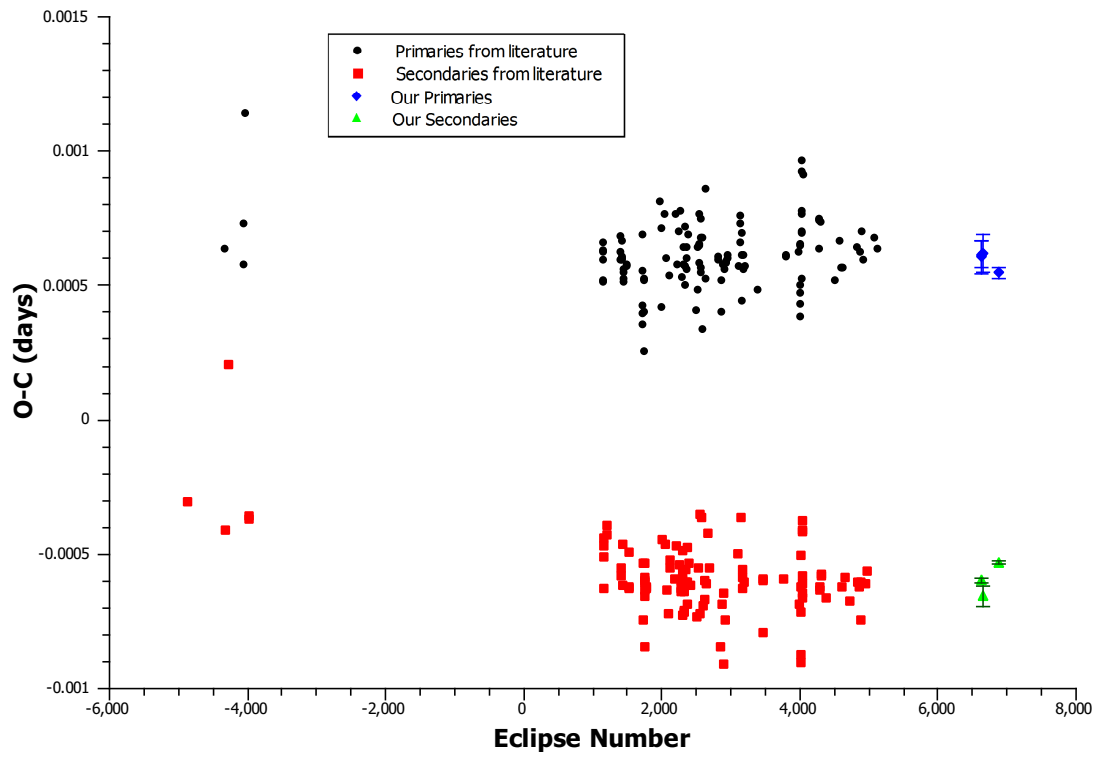Fig. 3.8.— HS 0705 spectral energy distribution

Fig. 3.9.— CM Draconis O-C with respect to a linear ephemeris computed from all eclipses

References

Aaronson, M., Huchra, J., Mould, J., Schechter, P. L., & Tully, R. B. 1982, ApJ, 258, 64

Applegate, J. H. 1992, ApJ, 385, 621

Backhaus, U., Bauer, S., Beuermann, K., et al. 2012, A&A, 538, AA84

Baraffe, I., & Chabrier, G. 1996, ApJ, 461, L51

Barlow, B. N., Wade, R. A., & Liss, S. E. 2012, ApJ, 753, 101

Beuermann, K., Breitenstein, P., Debski, B., et al. 2012, A&A, 540, AA8

Budaj, J. 2011, AJ, 141, 59

Çamurdan, C. M., Zengin Çamurdan, D., İbanoğlu, C. 2012, New Astronomy, 17, 325

Chabrier, G., Gallardo, J., & Baraffe, I. 2007, A&A, 472, L17

Charpinet, S., van Grootel, V., Reese, D., & Fontaine, G. 2008, A&A, 489, 377

Deeg, H. J., Ocaña, B., Kozhevnikov, V. P., et al. 2008, A&A, 480, 563

Depoy, D. L., Atwood, B., Byard, P. L., Frogel, J., & O'Brien, T. P. 1993, Proc. SPIE, 1946, 667

Drechsel, H., Heber, U., Napiwotzki, R., & Østensen, R. 2001, A&A, 379, 893

Eastman, J., Siverd, R., & Gaudi, B. S. 2010, PASP, 122, 935

Feiden, G. A., & Chaboyer, B. 2012, ApJ, 757, 42

For, B.-Q., Green, E. M., Fontaine, G., & Drechsel, D. 2010, ApJ, 708, 253

For, B.Q., Green, E. M., & Fontaine, G. 2010, ApJ, 329, 87

Han, Z., Podsiadlowski, P., Maxted, P. F. L., & Marsh, T. R. 2002, MNRAS, 336, 449

Han, Z., Podsiadlowski, P., Maxted, P. F. L., & Marsh, T. R. 2003, MNRAS, 341, 669

Irwin, J., Charbonneau, D., Berta, Z. K., et al. 2009, ApJ, 701, 1436

Kaplan, D. L. 2010, ApJ, 717, L108

Kelley, N., & Shaw, J. S. S. 2007, Journal of the Southeastern Association for Research in Astronomy, 1, 13

Kilkenny, D., O'Donoghue, D., Koen, C. & Lynas-Gray, A. E. 1998, MNRAS, 296, 329

Kilkenny, D., Keuris, S., Marang, F., et al. 2000, The Observatory, 120, 48

Kilkenny, D. 2011, MNRAS, 412, 487

Kraus, A. L., Tucker, R. A., Thompson, M. I., Craine, E. R., & Hillenbrand, L. A. 2011, ApJ, 728, 48

Kruspe, R., Schuh, S., & Traulsen, I. 2007, Information Bulletin on Variable Stars, 5796, 1

Lacy, C. H. 1977, ApJ, 218, 444

Lee, J. W., Kim, S.-L., Kim, C.-H., et al. 2009, AJ, 137, 3181

Lee, J. W., Hinse, T. C., Youn, J.-H., & Han, W. 2014, MNRAS, 445, 2331

Lenz, P., & Breger, M. 2004, The A-Star Puzzle, 224, 786

Liying, Z., & Shengbang, Q. 2010, Ap&SS, 329, 107

Lohr, M. E., Norton, A. J., Anderson, D. R., et al. 2014, A&A, 566, AA128

Mengel, J. G., Norris, J. & Gross, P. G. 1976, ApJ, 204, 488

Morales, J. C., Ribas, I., Jordi, C., et al. 2009, ApJ, 691, 1400

Nemeth, P., Kiss, L. L., & Sarneczky, K. 2005, Information Bulletin on Variable Stars, 5599, 15

Niarchos, P. G., Gazeas, K. D., & Manimanis, V. N. 2003, Interplay of Periodic, Cyclic and Stochastic Variability in Selected Areas of the H-R Diagram, 292, 129

Pulley, D., Faillace, G., Smith, D., & Owen, C. 2015, arXiv:1502.04366

Qian, S.-B., Zhu, L.-Y., Zola, S., et al. 2009, ApJ, 695, L163

Qian, S.-B., Zhu, L.-Y., Liu, L., et al. 2010, Ap&SS, 329, 113

Qian, S.-B., Zhu, L.-Y., Dai, Z.-B., et al. 2012, ApJ, 745, LL23

Qian, S.-B., Shi, G., Zola, S., et al. 2013, MNRAS, 436, 1408

Vučković, M., Aerts, C., Østensen, R., & Nelemans, G. 2007, A&A, 471, 605

Wood, J. H., & Saffer, R. 1999, MNRAS, 305, 820

Zellem, R. T., Lewis, N. K., Knutson, H. A., et al. 2014, ApJ, 790, 53